Ab initio equation of state of iron up to 1500 GPa

J. Bouchet
CEA, DAM, DIF, F-91297 Arpajon, France and LUTH UMR No. 8102, Observatoire de Paris, CNRS, Université Paris Diderot, 92195 Meudon, France

S. Mazevet
LUTH UMR No. 8102, Observatoire de Paris, CNRS, Université Paris Diderot, 92195 Meudon, France and CEA, DAM, DIF, F-91297 Arpajon, France

G. Morard and F. Guyot
Institut de Minéralogie et de Physique des Milieux Condensés, UMR No. 75-90, 140 Rue de Lourmel, 75015 Paris, France and Institut de Physique du Globe de Paris, 4 Place Jussieu, 75252 Paris, France

R. Musella
LUTH UMR No. 8102, Observatoire de Paris, CNRS, Université Paris Diderot, 92195 Meudon, France

(Received 14 May 2012; revised manuscript received 4 February 2013; published 4 March 2013)

Using *ab initio* molecular dynamics simulations, we calculate the equation of state of iron in the solid phase for both the hcp and bcc structures as well as the high-pressure melting curve up to 15 Mbars. We first find that the melting temperature increases up to 11 000 K at the highest pressures investigated following a semiempirical melting law over the entire pressure domain. We also investigate the stability of the bcc phase of iron beyond Earth's core conditions (3 Mbars) and find that the temperature at which the bcc phase is mechanically stabilized increases with density. Finally, we provide simple fits of these results for convenient use in the modeling of Earth-like exoplanets up to ten Earth masses, which requires accurate knowledge of the properties of iron up to 15 Mbars.

DOI: 10.1103/PhysRevB.87.094102 PACS number(s): 64.30.Ef, 91.60.Gf, 62.50.−p, 65.40.−b

I. INTRODUCTION

Several exoplanets with an average density similar to that of the Earth have been detected[1] in the past few years. Several studies have speculated[2,3] on the state of the iron core in these extrasolar objects, the so-called super-Earths. In order to better constrain the internal dynamics of these exoplanets, an accurate knowledge of the iron properties such as the equation of state (EOS) and melting curve is required. Previous theoretical studies on the high-pressure properties of iron focused on the Earth's core conditions[4–11] between 136 and 360 GPa and little is known in the domain relevant for super-Earths where internal pressures extend over 1500 GPa with temperatures remaining below 1 eV (1 eV = 11 604 K).[2,12,13] Properties of pure iron, which is a main component of these planetary cores, are thus needed under such extreme conditions.[14] Recently, calculations have been performed to study the relative stability of different crystal structures for pure Fe up to 100 TPa at 0 K (Refs. 15 and 16) and of temperature using the quasiharmonic approximation.[3]

The high-pressure melting curve of iron at conditions ranging from a few GPa to pressures relevant to the Earth's center (360 GPa) has previously been studied using shock waves (see e.g., Refs. 17–19) and laser-heated diamond anvil cells (see e.g., Refs. 20 and 21). The significant uncertainties in the experimental results obtained at such extreme pressures have generated intense activity on the theoretical side. Several predictions of the high-pressure melting curve of iron have been published over the past ten years using either classical potentials or a full quantum description of the electrons based on density functional theory (DFT).[22–27]

At pressures found at the Earth inner-core boundary (ICB), i.e., 330 GPa, Alfè *et al.*[23] obtained a melting temperature of 6400 K using thermodynamic integration. This initial calculation was later confirmed using the coexistence approach[22]. Recently, using Monte Carlo free-energy simulations, Sola and Alfè[24] obtained a melting temperature of 6900 K. We also note that using classical potentials fitted on *ab initio* simulations, Belonoshko *et al.*[25] predicted a melting point of 7100 K at this pressure. These predictions based on DFT, however, remain limited to the ICB conditions.

Using full *ab initio* molecular dynamics (AIMD) simulations based on DFT, we extend the high-pressure melting curve and the equation of state of iron over the entire pressure range relevant to the modeling of a super-Earth up to ten Earth masses (1500 GPa). We paid particular attention to the dynamical stability of the bcc phase at high pressures as this potentially affects the predictions regarding the melting temperatures. We also provide simple analytical fits to these results to facilitate their use in planetary modeling.

II. SIMULATION METHOD

Simulations were performed using the *ab initio* package ABINIT.[28–30] The calculations used the projector augmented wave method[31,32] for the calculation of the electronic structure and the generalized gradient approximation according to the parametrization of Perdew, Burke, and Ernzerhof for the exchange-correlation energy and potential.[33] Details of the pseudopotential generation as well as a comparison for the 300-K isotherm with experimental data can be found in Ref. 34. We generated two pseudopotentials with $3s$, $3p$, $3d$,

and 4*s* states as valence electrons and cutoff radii of 2.1 and 1.7 Ha. The pseudopotential with the lowest radius was used at high pressure to avoid overlapping between the atomic spheres. At the highest density considered in this work (20 g/cm^3) the interatomic distance between first nearest neighbors is about 3.44 and 3.51 for bcc and hcp (with $c/a = 1.6$), respectively.

The AIMD simulations were performed using a cutoff energy for the plane-wave basis chosen equal to 350 and 540 eV for the 2.1- and 1.7-Ha radius pseudopotentials, respectively. We performed simulations in the isokinetics ensemble where the number of particles, volume, and temperature are held fixed during the simulation. In this simulation ensemble, the temperature is kept constant by rescaling the velocities at each time step. For the EOS, we performed simulations on both the hcp and bcc structures as these two phases are candidates for the stable phase of iron at high pressure.[11,35,36] For both hcp and bcc phases, we performed simulations with supercells of 128 ($4 \times 4 \times 4$ unit cells) atoms at the Γ point. The former simulation parameters correspond to the ones previously used to calculate the elastic constants with the AIMD method.[37] As will be shown below, we find that simulations need to be performed using at least 128 atoms in order to obtain convergence of the various physical properties calculated in the present work. For the hcp phase, we used 128 atoms in the simulation cell and, as for the bcc phase, checked convergence of the physical quantities against particle number by using up to 512 atoms. The two radius pseudopotentials were tested at the highest density to estimate the effect of the overlapping on the pressure; the difference was around 0.8%. To obtain the melting curve of bcc iron we used a heat until it melts (HUM) approach with supercells of 128 atoms and a two-phase approach[38] with supercells of 108 and 256 atoms.

III. THE AIMD SIMULATIONS FOR hcp AND bcc

In Fig. 1 we show the span in pressure and temperature over which we performed the AIMD simulations for both the hcp and bcc phases. We simulated properties along several isochores for densities ρ ranging from 10 to 20 g/cm^3 and for temperatures extending from 500 to 14 000 K. We focused on four isochores at $\rho = 13.5$, 16, 18, and 20 g/cm^3. For the hcp phase we used a c/a ratio of 1.6. There has been some debate about the temperature dependence of this value. Earlier findings show a strong increase, with values up to 1.7 at ICB conditions,[5,39] which is later contradicted by AIMD simulations[10] and linear response calculations.[9] At chosen pressure-temperature points we looked at the stress components and changed the c/a ratio to obtain the equilibrium value. Even at the highest pressures considered here we find only a small dependence on temperature of the c/a ratio (less than 1%), with no effect on the pressure. This confirms and extends the previous results at ICB conditions.[9,10] All the hcp pressure-temperature points in Fig. 1 are given for a c/a ratio of 1.6.

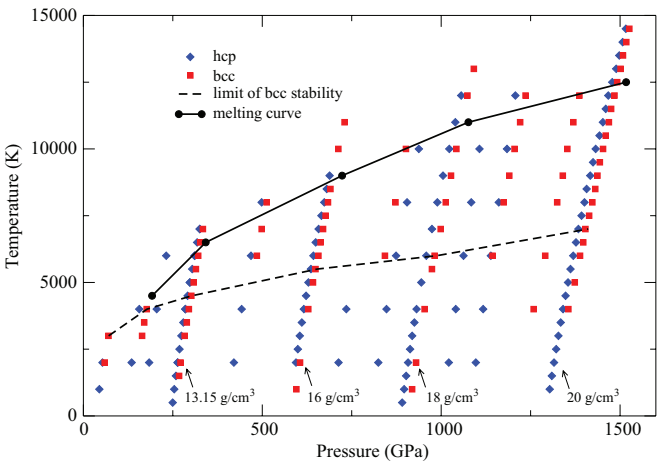

FIG. 1. (Color online) Pressure-temperature span over which AIMD simulations have been performed. The symbols indicate the different simulation runs. See the text for details.

A. Elastic bcc stability

Several *ab initio* studies performed so far at the ICB conditions point to a possible stable bcc phase for temperatures approaching melting.[11,25,37,40,41] At normal conditions, the stable phase of iron is a magnetically stabilized bcc phase. Iron turns into a nonmagnetic fcc phase above 1000 K, a temperature comparable to the Curie temperature. Upon a pressure increase, the bcc phase is stabilized by magnetism up to 14 GPa. Above this pressure and for moderate temperature (below 1000 K), iron turns into a nonmagnetic hcp phase up to the highest pressure explored so far experimentally. The situation is more controversial at higher pressures and temperatures. Various experimental measurements performed using either static or dynamic compression have been interpreted as evidence for a double hcp (dhcp) phase at temperatures between 2000 and 4000 K and pressures above 20 GPa and a nonmagnetic bcc phase at pressure close to the ICB conditions and temperatures above 5000 K.[11] It is important, however, to note that these experimental results lack reproducibility and thus no post hcp phase has been unambiguously identified.[42]

The situation has been barely clarified using *ab initio* simulations. It is well known that at 0 K, the phonon spectrum of iron exhibits soft modes[11,43] and is unstable towards a tetragonal distortion.[44] While AIMD simulations have indicated that the bcc phase is stabilized at temperatures above 4000 K at ICB conditions,[11] it has not been possible to identify the most stable phase between the hcp and bcc phases. The difficulty directly comes from the methods available to obtain the free energy of these two phases combined with the instability of the bcc phase at zero temperature. This issue has been investigated in great details by Vocadlo *et al.*[40] For conditions corresponding to the ICB, they found that the difference in free energy between the two phases remains within the error bar of the method. To obtain this result, Vocadlo *et al.*[40] used thermodynamics integration. This uncertainty, which in turn results in maintaining a deep mystery about the iron solid phase present in the Earth;s inner core, is somewhat tempered by the fact that the Earth's core is likely not composed of pure iron but rather of an iron-nickel alloy for which a bcc phase is anticipated at these conditions.[40,45–47] However, the presence of other elements such as silicon or oxygen does not allow that major issue to really be resolved. Moreover, complicating the issue of relative stabilities of bcc and hcp phases, there are questions about the intrinsic stability of the bcc phase of iron.[37]

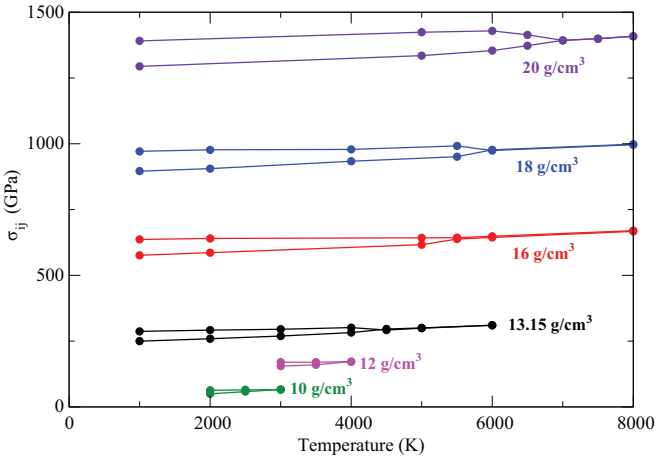

FIG. 2. (Color online) Variation of the stress components as a function of temperature along six isochores of bcc iron.

In order to study the elastic stability of the bcc phase, we extracted the stress components in that phase at various temperatures and densities, as calculated in the AIMD simulations. As pointed out in Refs. 11 and 40, inspection of the stress components can give an indication of the density-temperature range over which a given phase is mechanically stable. Figure 2 shows the variation of the stress components in temperature over six different isochores ($\rho = 10$, 12, 13.15, 16, 18, and 20 g/cm^3). The values of the stress components given in Fig. 2 correspond to averages obtained over the whole molecular dynamics trajectories. The minimum temperature for stability of the bcc phase has been reported as a function of pressure in Fig. 1. At the lowest density, we see that the bcc cell is in hydrostatic equilibrium for temperatures above 3000 K and above 4500 K at the ICB conditions (330 GPa, $\rho = 13.15$/g/cm^3). This confirms earlier findings[11] that the bcc cell becomes stable above temperatures of about 3000 K at conditions of the ICB. Using self-consistent *ab initio* lattice dynamical calculations that go beyond the quasiharmonic approximation by taking into account the temperature effects on the phonon spectra, Luo *et al.*[48] reached similar conclusions. Recently Kong *et al.*[49] extracted the phonon spectrum of pure iron using molecular dynamics and an embedded-atom method (EAM) empirical potential. They also found that the bcc structure becomes stable close to the melting temperature.

Inspection of Fig. 1 shows that the temperature at which the bcc phase is stable increases as a function of pressure, a result in agreement with recent calculations of Kong *et al.*,[49] which studied the dynamical stability of pure iron using molecular dynamics and an EAM empirical potential. We see that the bcc phase remains unstable up to a temperature of 7000 K at the highest density investigated ($\rho = 20$ g/cm^3). This also shows that the situation up to 1500 GPa (15 Mbars) remains rather similar to the one found at ICB conditions with a bcc phase stabilizing as temperature approaches the melting temperature. This also suggests that the instability of the bcc phase may become even more pronounced as the density increases, thus requiring higher electronic temperatures to stabilize it. While this formally needs to be verified by calculating the electronic temperature dependence of the phonon spectrum, this may be reminiscent of what was already found for other metals such as Al and Au.[50] For these systems, it was shown that an increase in the electronic temperature correlated with the hardening of the phonon spectrum. A scenario compatible with the data at hand for iron would thus be that a significant increase in electronic temperature could stabilize the bcc phase at high temperature, with higher temperatures being required as density increases and the instability at 0 K being more pronounced.

The variations of the stress components as a function of pressure thus indicate that the bcc phase becomes elastically stable above a given temperature over the entire pressure range considered. They do not indicate, however, which is the most stable phase of iron at those conditions. This would formally require the calculation of the free energy,[40] which is beyond the scope of the present study. For super-Earth modeling the questions regarding the stability of the bcc phase are first whether the nonmagnetic bcc phase becomes the most stable phase as pressure increases by up to five times the ones found at ICB conditions and second whether this phase should be considered when calculating the high-pressure melting curve of iron. It is potentially determinant to use the proper phase for the calculation of the high-pressure melting curve as the substitution of a metastable phase in its calculation could lead to a significant underestimation of the melting temperature. To address these issues, we thus calculate bulk melting temperatures for both phases over the entire pressure domain investigated.

B. High-pressure melting curve

To extend the calculation of the high-pressure melting curve of iron to pressures encountered in super-Earths of up to ten Earth masses, we employed direct AIMD simulations. We performed both direct bulk melting, i.e., the HUM approach, and two-phase simulations. In the former, a simulation cell initially corresponding to a single solid phase is gradually heated until melting occurs. In the latter, liquid and solid simulation cells are initially brought into contact. The simulation is then performed in the isokinetics ensemble where the temperature is held fixed and until the sample equilibrates in either the liquid or the initial solid phase. We favored this simulation method over thermodynamic integration as the latter requires finding a reference system to extract the free energy of the phase at hand.[10,51]

Figure 3 shows the melting temperatures obtained with the HUM method when considering the bcc or hcp phases with varying numbers of atoms. When considering only 54 atoms and four **k** points as used in previous studies,[36,37] we obtain significantly different melting temperatures between the two phases. These differences disappear as soon as the number of atoms used in the simulation cell is increased up to 128 atoms and more. This suggests that AIMD simulations should be performed with at least 128 atoms in the simulation cell when considering two-phase simulation. This also indicates that the high-pressure melting temperature does not significantly depend on the solid phase used. This result is consistent with the small free-energy difference found between the two phases at ICB conditions.[11,35,41] The result shown here goes a step further and suggests that the difference in free energy between the two phases remains modest up to the highest pressures considered. This shows that the high-pressure melting tem-

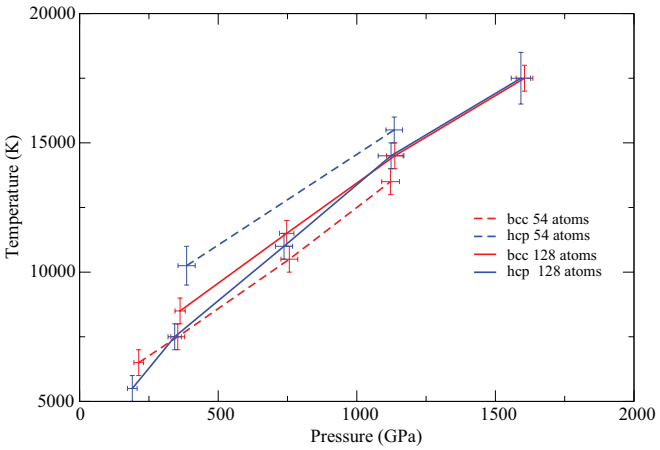

FIG. 3. (Color online) Bulk melting temperature as a function of pressure for the hcp and bcc phases. The number of atoms used in the simulation cell is indicated on the graph.

perature will not depend on the solid phase chosen in the two-phase simulation approach for the entire pressure domain investigated here.

Due to the only small differences found by the HUM method between melting curves of the hcp and bcc phases (see also Ref. 27), we used the bcc structure in two-phase simulations. The results are shown in Fig. 4 and compared to previous calculations performed at conditions corresponding to the ICB. Alfè *et al.*[10] used thermodynamic integration, while Belonoshko *et al.*[25] used the two-phase method with an EAM potential fitted at high pressure to *ab initio* calculations. Although differences exist between the results obtained by these two groups, Alfè *et al.*[51] have shown how to reconcile the EAM results with results based on free energy.

We thus used the two-phase approach with cells containing 108 (2×54) and 256 (2×128) atoms. As noted previously for aluminum,[52] the discrepancies between the results obtained using cells of two different sizes increase with pressure. We find a difference of about 7% in the resulting melting temperature at the highest pressure considered here, while for

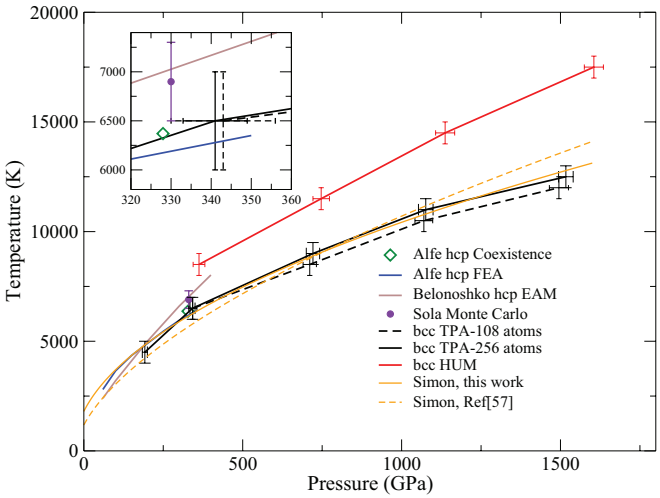

FIG. 4. (Color online) Variation of the melting temperature of bcc iron as a function of pressure using two-phase simulations.

the lowest pressures the difference is within the error bars. At the terrestrial ICB conditions, the melting point is in excellent agreement with the most recent calculations obtained using the coexistence approach and a larger supercell of 1000 atoms.[22] This gives us strong confidence in the reliability of the melting curve calculated using this approach with 256 atoms in the simulation cell, in spite of the resulting larger error bar on the melting temperature calculated. As an hcp structure was used in Ref. 22, the result found at ICB conditions also confirms that the melting temperatures obtained using either a bcc or hcp structure are within the error bar of the simulation method.

The two-phase approach leads to melting temperatures almost constantly increasing as a function of pressure. As expected, we observe a strong reduction of the melting temperature between the HUM and the two-phase approach. The slope, however, is slightly smaller when calculated with the two-phase approach and yields a melting temperature at 1500 GPa of about twice the one obtained at terrestrial ICB conditions. This contrasts with findings in systems such as Na and H where maxima in the melting curve were identified at high pressures.[53,54] The melting curve obtained in the present study can be compared usefully with existing models of planetary cores.[55] The melting curve exhibits a significantly steeper slope than planetary adiabatic temperature profiles currently calculated for super-Earths. As explained by Morard *et al.*,[27] this suggests that the presence of liquid iron in the cores of super-Earths is not likely in planets of masses superior to Earth's mass.[27] The calculated melting curve of iron has also been reported in Fig. 1 together with the domain of elastic stability of the bcc phase. To estimate the effect of the overlapping between atomic spheres, HUM and two-phase approach calculations were performed with the 2.1-Ha radius pseudopotential. We do not find a difference in the melting temperature with the HUM method, but with the two-phase approach the melting temperature is 2000 K higher at 20 g/cm^3. This is certainly a direct consequence of the wrong description of the liquid part where the overlapping is the largest.

In order to facilitate further planetary modeling, we fitted the melting temperatures obtained in the present study above 3 Mbars and together with the results of Alfe *et al.*[10,51] below 3 Mbars using the semiempirical Simon melting law,[14] which links melting temperature to pressure according to

$$\frac{P - P_0}{a} = \left(\frac{T_m}{T_0}\right)^c - 1, \qquad (1)$$

where a and c are empirical parameters. Simulations results are well reproduced over the entire pressure range using $a = 31.3$ GPa and $c = 1.99$. Murphy *et al.*[56] used a measured phonon density of states at 300 K between 30 and 151 GPa to determine the vibrational free energy and mean-square displacement of atoms. Then they determine the melting temperature and proposed a Simon law. We extrapolated their results to the pressure domain considered here for comparison (see Fig. 4).

C. Thermodynamic properties extracted directly from AIMD

The variation of pressure P and internal energy U as a function of temperature allows us to calculate the specific heat C_V and αK_T, the product of the isobaric thermal expansivity

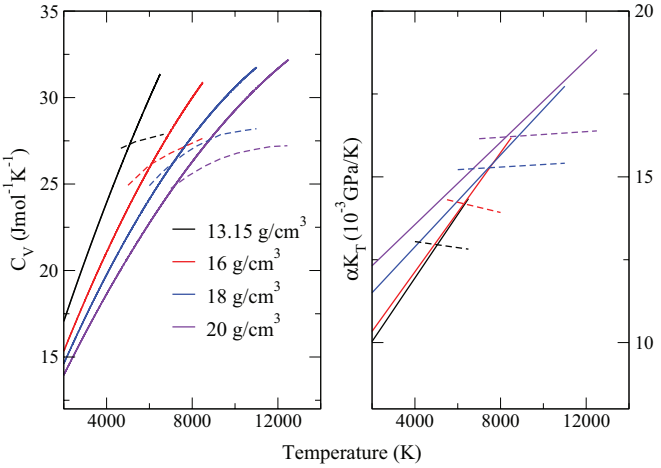

FIG. 5. (Color online) Specific heat at constant volume C_V (left) and αK_T (right) for hcp (continuous curves) and bcc (dashed curves) iron along four isochores as a function of temperature (up to the melting temperature). For the bcc phase we only report the values in the elastic stability domain defined in Fig. 1.

and the isothermal bulk modulus. They are defined as $C_V = (\partial U/\partial T)_V$ and $\alpha K_T = (\partial P/\partial T)_V$, respectively. They are reported in Fig. 5 for the four isochores reported in Fig. 1.

The specific heat C_V shows an almost linear increase with temperature in the hcp phase, while in the bcc phase a maximal value close to the classical value of 25 J mol^{-1} K^{-1} is reached. As pressure is increased at a given temperature, C_V decreases due to the suppression of electronic excitations and anharmonicity. The same behavior is observed for αK_T. This quantity is sometimes considered to be independent of the temperature, which means that the thermal pressure is linear in T.[57] We clearly observe this quasiharmonic behavior for the bcc phase, but not for the hcp phase. Similar values for αK_T are reported by Alfe *et al.*[10] at the ICB pressure range.

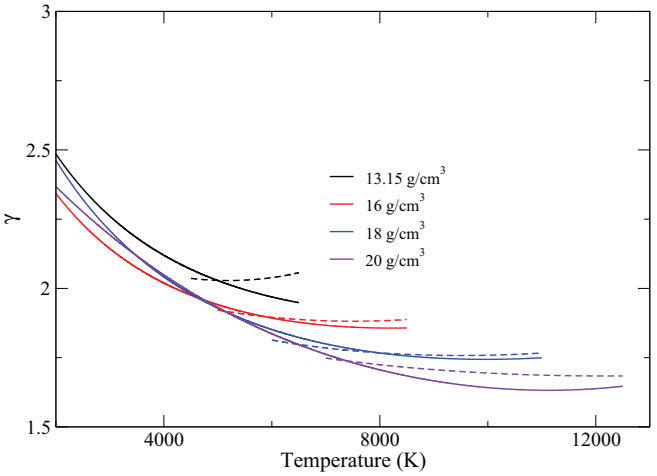

FIG. 6. (Color online) Grüneisen parameter γ for hcp (continuous curves) and bcc (dashed curves) iron along four isochores as a function of temperature (up to the melting temperature). For the bcc phase we only report the values in the elastic stability domain defined in Fig. 1.

From these two quantities, it is easy to obtain the thermodynamic Grüneisen parameter γ defined as

$$\gamma = \frac{\alpha K_T V}{C_v}. \quad (2)$$

The variation of the Grüneisen parameter is reported in Fig. 6. For both structures, γ decreases as density increases. At high temperatures, where the bcc phase is elastically stable, the temperature dependence of γ is really weak. We find similar values for both structures, ranging from 2.0 at the lowest densities to 1.7 at the highest. Using a measured phonon density of states, Murphy *et al.*[58] found an ambient pressure vibrational Grüneisen parameter $\gamma_{\text{vib}} = 2.0 \pm 0.1$ for hcp iron. Using the quasiharmonic approximation, Sha and Cohen[9] show a rapid decrease in temperature of the Grüneisen parameter for ϵ-Fe with values lower than reported here, between 2.2 and 1.0, depending on temperature and density.

IV. EQUATIONS OF STATE OF hcp AND bcc IRON AT VERY HIGH PRESSURES

In the past decade, *ab initio* calculations have been extensively used to study the thermal properties of iron and build reliable equations of state of iron at the temperature and pressure of the Earth's core. Sha and Cohen[8,9] used the quasiharmonic approximation to study bcc and hcp structures of iron. Alfè *et al.* used the quasiharmonic approximation and thermal integration to take into account the anharmonic effect to study hcp Fe. Belonoshko *et al.*[36] used AIMD simulations to build an equation of state of bcc iron. In the adiabatic approximation, the Helmholtz free energy $F(V,T)$ for a solid can be expressed as[59]

$$F = E(V) + F_{\text{harm}}(V,T) + F_{\text{anh}}(V,T) + F_{el}(V,T), \quad (3)$$

where E is the potential part of the free energy at zero temperature. Here $F_{\text{harm}}(V,T)$ is the harmonic part of the vibrational free energy that can be obtained using linear response theory and the quasiharmonic approximation for the ion motion, $F_{\text{anh}}(V,T)$ represents the correction due to anharmonicity, and $F_{el}(V,T)$ represents the electronic contribution. The adiabatic approximation is useful when using, for example, lattice dynamics. When using AIMD simulations as in the work here, we calculate the total pressure for the relaxed structure at any given density and temperature. As the ions are propagated using the classical equation of motion, this is justified only for temperatures above the Debye temperature where the ionic motion can be considered as classical. In contrast, anharmonic effects are directly included in the calculations of the total pressure. As the simulations are performed using finite-temperature density functional theory, the effect of the electronic contribution on the resulting pressure is also directly included.

Several functional forms are used to parametrize the zero-temperature EOS also referred to as the cold curve. Here we used the Holzapfel form[60] as it provides the correct Thomas-Fermi limit at infinite compression.[36] As such, it is formally more appropriate than the Vinet or Birch-Murnaghan functionals to cover the compression range studied here. Within this parametrization, the pressure is given as

$$P(V) = 3K_0X^5(1-X)\exp[c_0(1-X)][1+c_2X(1-X)], \quad (4)$$

with $X = (V/V_0)$, $c_0 = -\ln(3K_0/P_{FG0})$, $P_{FG0} = 1003.6(Z/V_0)^{5/3}$, and $c_2 = 3/2(K' - 3) - c_0$, where V_0 and K_0 are the molar volume and bulk modulus at normal conditions. Here P_{FGO} is given in GPa and V_0 in cm^3/mole.

Similarly to Ref. 36, we choose the Einstein model to describe the harmonic contribution to the pressure. The thermal contribution to the pressure can thus be parametrized as

$$P_{\text{harm}} = \gamma E_{\text{harm}}/V, \tag{5}$$

with

$$E_{\text{harm}} = 3nR\left[\Theta/2 + \frac{\Theta}{\exp(\Theta/T) - 1}\right], \tag{6}$$

$$\gamma = \gamma_\infty + (\gamma_0 - \gamma_\infty)(V/V_0)^\beta, \tag{7}$$

$$\Theta = \Theta_0 (V/V_0)^{-\gamma_\infty} \exp\left[\frac{\gamma_0 - \gamma_\infty}{\beta}[1 - (V/V_0)^\beta]\right], \tag{8}$$

where γ is the Grüneisen parameter, γ_0 and γ_∞ are its values at ambient conditions and infinite compression following the Al'tshuler *et al.* form,[61] Θ is the Einstein temperature, R is the gas constant, and n is the number of atoms, one in the present case. In these two relations and as for the cold curve, Θ_0, γ_∞ γ_0, and β are fitting parameters and formally do not carry any physical meaning. Following Refs. 62 and 36, we used for the anharmonic and electronic terms P_a and P_e, respectively,

$$P_a = \frac{3R}{2V} m a_0 x^m T^2 \tag{9}$$

and

$$P_e = \frac{3R}{2V} g e_0 x^g T^2. \tag{10}$$

Since these two terms have the same temperature dependence, we finally used only one expression P_{ae}, which thus contains both contributions. This has no impact on the quality of the fitting procedure.

To fit all the (P,V,T) points shown in Fig. 1, we considered first fitting globally the data using the sum of the Holzapfel, Einstein, and electronic-anharmonic forms. We also considered removing the cold curve contribution first and fitting the thermal pressure on the remaining pressure in a second step. Overall, as our primary concern here is to summarize our data in a simple analytical form, we find that a global fit provides the desired accuracy. Note that for the bcc phase we used only the V and T points where the phase is considered to be dynamically stable.

Over the whole pressure and temperature range explored here, the *ab initio* pressures are reproduced within less than 1% when using the set of parameters presented in Table I (see Fig. 7). To check the quality of the fit, we performed additional AIMD calculations for various values of V and T; the difference between the calculated pressures and the fitted

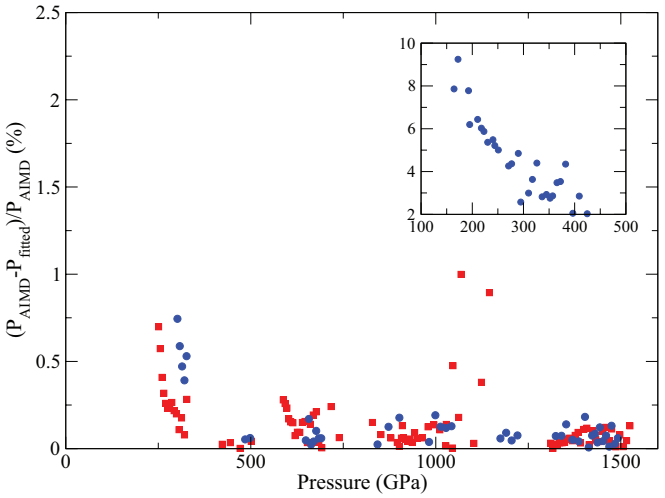

FIG. 7. (Color online) Difference (in percent) between computed pressures (AIMD) and fitted ones for hcp and bcc phases. The inset shows the result of our bcc fit with the P,V,T points of Ref. 36.

ones was less than 1%. While it is customary to associate physical quantities with these fitting parameters, we stress that the values obtained here are relevant only within the complete set of parameters used to fit the input data within a given error bar. As such, these parameters do not bear any physical meaning when taken individually as several parameter sets can provide the required fit within a few percent.

We now compare our EOS with the previous one proposed by Belonoshko *et al.*[36] for the bcc phase at conditions close to the ICB. This EOS was also obtained using AIMD simulations, but used smaller supercells containing 54 atoms. We used our EOS to reproduce the pressures obtained in these calculations (see the inset of Fig. 7). We observe large discrepancies between the computed and fitted pressures at low pressures, around 7%. The differences drop to around 2% at 400 GPa. This can be explained by the fact that there is a difference of several GPa between supercells of 54 and 128 atoms simulated in the same conditions as indeed discussed by Belonoshko *et al.*[36] The pressure differences between simulations cells of 128 and 250 atoms are less than 1%, which stresses that a supercell of at least 128 atoms is necessary. We also note that to obtain our EOS, we only used P,V,T points in the stability domain of bcc, starting above 4000 K at 250 GPa. It is therefore not surprising to find the largest discrepancies in a domain of pressures not covered by our input data.

As also noticed by Belonoshko for inner core P-T conditions, we also observe that the anharmonic-electronic contribution to the pressure is almost negligible for the bcc phase (see the value of a_0 in Table I) in spite of the high temperatures considered here. This contrasts with the hcp

TABLE I. Set of parameters resulting from our fitting procedure for bcc and hcp iron.

Structure	V_0 (cm^3/mole)	K_0 (GPa)	K_0' (GPa)	Θ_0 (K)	γ_0	β	γ_∞	a_0 (K^{-1})	m
bcc	6.544	199.520	5.070	451.500	2.418	0.491	0.561	7.623×10^{-8}	3.394
hcp	6.290	253.844	4.719	44.574	1.408	0.826	0.827	2.121×10^{-4}	1.891

phase, where anharmonic effects are more important and contribute significantly to the pressure. This is in agreement with the behavior shown in Fig. 5, where the classical limit is recovered in bcc iron and not in hcp iron.

V. OTHER THERMODYNAMIC QUANTITIES OF bcc AND hcp IRON AT VERY HIGH PRESSURES

The fit obtained in the preceding section allows us to deduce several thermodynamic quantities such as the isothermal bulk modulus and the isobaric volume expansion coefficient defined as

$$K_T = -V\left(\frac{\partial P}{\partial V}\right)_T, \tag{11}$$

$$\alpha = \frac{1}{V}\left(\frac{\partial V}{\partial T}\right)_P. \tag{12}$$

We further note that these quantities are derivative of P, V, and T and do not depend on the individual parameters obtained from the fit. Figure 8 shows the behavior of these quantities for bcc iron in its elastic stability domain and for hcp iron. The isothermal bulk moduli obtained for the bcc and hcp phases are rather close over the whole range of pressure and temperature considered here. Similar conclusions can be obtained for the isobaric thermal expansivity. The temperature dependence, however, is much more pronounced for the hcp phase than in the bcc phase. The isobaric thermal expansivity decreases strongly with increasing pressure in both structures. This behavior was observed in diamond-anvil-cell experiments[63] for the hcp phase at lower pressures. For comparison, we also show the values obtained by Alfe *et al.*[10] In the present work, the Helmholtz free energy was obtained by calculating separately the cold curve and the harmonic and anharmonic contributions. Despite the fact that we used a different approach to deduce the free energy, we obtain rather similar results. We also find good agreement at 200 and 300 GPa with the values obtained with the EOS of Dewaele *et al.*[62] for the hcp phase. This EOS is based on experimental compression data at room temperature, Hugoniot data,[64] and *ab initio* modeling.[10] The close agreement that we observe at low pressures for the thermal expansivity gives confidence in our high-pressure predictions.

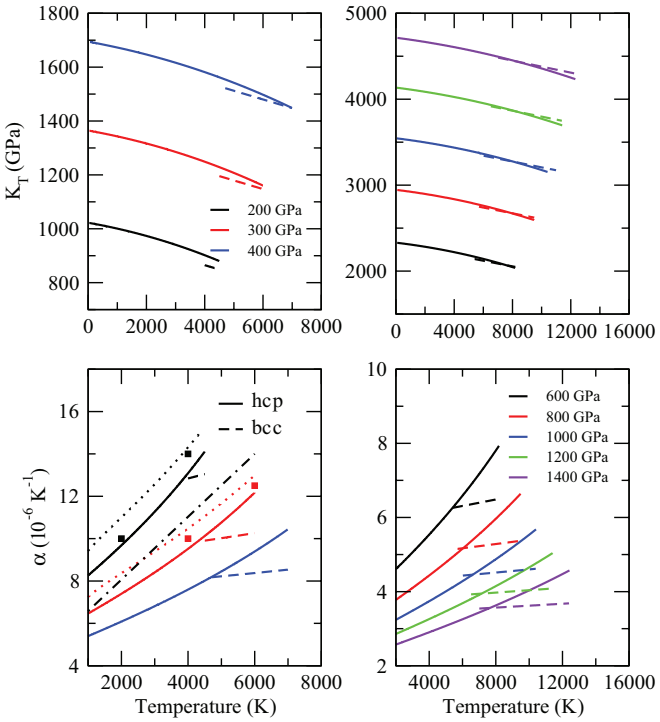

FIG. 8. (Color online) Isothermal bulk modulus and volume expansion coefficient of hcp and bcc iron as a function of temperature and for several pressures (left panels, 200–400 GPa; right panels, 600–1400 GPa). The dotted curves are the results of Ref. 62, the squares are the results of Ref. 10, and the dot dashed line is the result of Ref. 9 for the volume expansion coefficient of hcp Fe.

VI. CONCLUSION

Using *ab initio* molecular dynamics simulations, we calculated the equation of state of iron in the solid phase for both hcp and bcc structures as well as the high-pressure melting curve up to 15 Mbars. We also investigated the elastic stability of the bcc phase and found that the temperature above which the bcc phase is mechanically stabilized increases with density. Finally, we provided simple fits of these results for convenient use in the planetary modeling.

[1] J. P. Beaulieu *et al.*, Nature (London) **439**, 437 (2006).
[2] D. Valencia, R. J. O'Connell, and D. Sasselov, Icarus **181**, 545 (2006).
[3] L. Stixrude, Phys. Rev. Lett. **108**, 055505 (2012).
[4] L. Stixrude and R. E. Cohen, Science **267**, 1972 (1995).
[5] E. Wasserman, L. Stixrude, and R. E. Cohen, Phys. Rev. B **53**, 8296 (1996).
[6] G. Steinle-Neumann, L. Stixrude, and R. E. Cohen, in *Introduction to the Physics of the Earth's Interior*, edited by V. Dehant, K. Creger, S.-I. Karato, and S. Zatman, Earth's Core Lattice Dynamics, Structure, Rotation, Geodynamics Series Vol. 31 (American Geophysical Union, Washington, DC, 2003).
[7] X. Sha and R. E. Cohen, Phys. Rev. B **74**, 214111 (2006).
[8] X. Sha and R. E. Cohen, Phys. Rev. B **73**, 104303 (2006).
[9] X. Sha and R. E. Cohen, Phys. Rev. B **81**, 094105 (2010).
[10] D. Alfè, G. D. Price, and M. J. Gillan, Phys. Rev. B **64**, 045123 (2001).
[11] L. Vocadlo, D. Alfè, M. J. Gillan, I. G. Wood, J. P. Brodholt, and G. D. Price, Nature (London) **424**, 536 (2003).
[12] S. Seager, M. Kuchner, C. A. Hier-Majumder, and B. Militzer, Astrophys. J. **669**, 1279 (2007).
[13] D. C. Swift, J. H. Eggert, D. G. Hicks, S. Hamel, K. Caspersen, E. Schwegler, G. W. Collins, N. Nettelmann, and G. J. Ackland, Astrophys. J. **744**, 59 (2012).
[14] J. P. Poirier, *Introduction to the Physics of the Earth's Interior* (Cambridge University Press, Cambridge, 2004).

[15]C. J. Pickard and R. J. Needs, J. Phys.: Condens. Matter **21**, 452205 (2009).
[16]S. Cottenier, M. Probert, T. V. Hoolst, V. V. Speybroeck, and M. Waroquier, Earth Planet. Sci. Lett. **312**, 237 (2011).
[17]J. M. Brown and R. G. McQueen, J. Geophys. Res. **91**, 7485 (1986).
[18]J. H. Nguyen and N. C. Holmes, Nature (London) **427**, 339 (2004).
[19]C. S. Yoo, N. C. Holmes, M. Ross, D. J. Webb, and C. Pike, Phys. Rev. Lett. **70**, 3931 (1993).
[20]R. Boehler, Nature (London) **363**, 534 (1993).
[21]G. Shen, H. K. Mao, R. J. Hemley, T. S. Duffy, and M. L. Rivers, Geophys. Res. Lett. **25**, 373 (1998).
[22]D. Alfè, Phys. Rev. B **79**, 060101 (2009).
[23]D. Alfè, G. D. Price, and M. J. Gillan, Phys. Rev. B **65**, 165118 (2002).
[24]E. Sola and D. Alfè, Phys. Rev. Lett. **103**, 078501 (2009).
[25]A. B. Belonoshko, R. Ahuja, and B. Johansson, Phys. Rev. Lett. **84**, 3638 (2000).
[26]A. Laio, S. Bernard, G. L. Chiarotti, S. S. Scandolo, and E. Tosatti, Science **287**, 1027 (2000).
[27]G. Morard, J. Bouchet, D. Valencia, S. Mazevet, and F. Guyot, High Energy Density Phys. **7**, 141 (2011).
[28]The ABINIT code is a common project of the Catholic University of Louvain (Belgium), Corning Incorporated, CEA (France), and other collaborators (http://www.abinit.org).
[29]X. Gonze, J.-M. Beuken, R. Caracas, F. Detraux, M. Fuchs, G.-M. Rignanese, L. Sindic, M. Verstraete, G. Zerah, F. Jollet, M. Torrent, A. Roy, M. Mikami, P. Ghosez, J.-Y. Raty, and D. C. Allan, Comput. Mater. Sci. **25**, 478 (2002).
[30]F. Bottin, S. Leroux, A. Knyazev, and G. Zérah, Comput. Mater. Sci. **42**, 329 (2007).
[31]P. E. Blöchl, Phys. Rev. B **50**, 17953 (1994).
[32]M. Torrent, F. Jollet, F. Bottin, G. Zerah, and X. Gonze, Comput. Mater. Sci. **42**, 329 (2008).
[33]J. P. Perdew, K. Burke, and M. Ernzerhof, Phys. Rev. Lett. **77**, 3865 (1996).
[34]A. Dewaele, M. Torrent, P. Loubeyre, and M. Mezouar, Phys. Rev. B **78**, 104102 (2008).
[35]A. B. Belonoshko, R. Ahuja, and B. Johansson, Nature (London) **424**, 1032 (2003).
[36]A. B. Belonoshko, P. I. Dorogokupets, B. Johansson, S. K. Saxena, and L. Koci, Phys. Rev. B **78**, 104107 (2008).
[37]L. Vocadlo, Earth Planet. Sci. Lett. **254**, 227 (2007).
[38]A. B. Belonoshko, Geochim. Cosmochim. Acta **58**, 4039 (1994).
[39]G. Steinle-Neumann, L. Stixrude, R. E. Cohen, and O. Gulseren, Nature (London) **413**, 57 (2001).
[40]L. Vocadlo, I. G. Wood, and M. J. Gillan, Phys. Earth Planet. Inter. **170**, 52 (2008).
[41]A. B. Belonoshko, S. Arapan, and A. Rosengren, J. Phys.: Condens. Matter **23**, 485402 (2011).
[42]A. Dewaele, M. Mezouar, N. Guignot, and P. Loubeyre, Phys. Rev. Lett. **104**, 255701 (2010).
[43]P. Söderlind, J. A. Moriarty, and J. M. Wills, Phys. Rev. B **53**, 14063 (1996).
[44]L. Stixrude, R. E. Cohen, and D. Singh, Geophys. Res. Lett. **22**, 125 (1995).
[45]A. B. Belonoshko, A. Rosengren, L. Burakovsky, D. L. Preston, and B. Johansson, Phys. Rev. B **79**, 220102 (2009).
[46]A. S. Cote, L. Vocadlo, and J. P. Brodholt, Geophys. Res. Lett. **35**, L05306 (2008).
[47]L. S. Dubrovinsky, N. A. Dubrovinskaia, O. Narygina, I. Kantor, A. Kuznetzov, V. B. Prakapenka, L. Vitos, B. Johansson, A. S. Mikhaylushkin, S. I. Simak, and I. A. Abrikosov, Science **316**, 1880 (2007).
[48]W. Luo, B. Johansson, O. Eriksson, S. Arapan, P. Souvatzis, M. I. Katsnelson, and R. Ahuja, Proc. Natl. Acad. Sci. USA **107**, 9962 (2010).
[49]L. T. Kong, J. F. Li, Q. W. Shi, H. J. Huang, and K. Zhao, Europhys. Lett. **97**, 56004 (2012).
[50]V. Recoules, J. Clerouin, G. Zerah, P. M. Anglade, and S. Mazevet, Phys. Rev. Lett. **96**, 055503 (2006).
[51]D. Alfè, M. J. Gillan, and G. D. Price, J. Chem. Phys. **116**, 7127 (2002).
[52]J. Bouchet, F. Bottin, G. Jomard, and G. Zérah, Phys. Rev. B **80**, 094102 (2009).
[53]S. A. Bonev, E. Schwegler, T. Ogitsu, and G. Galli, Adv. Comput. Methods Sci. Eng. A **4**, 1122 (2005).
[54]J.-Y. Raty, E. Schwegler, and S. A. Bonev, Nature (London) **449**, 448 (2007).
[55]G. Morard, D. Andrault, N. Guignot, C. Sanloup, M. Mezouar, S. Petitgirard, and G. Fiquet, Earth Planet. Sci. Lett. **272**, 620 (2008).
[56]C. A. Murphy, J. Jackson, W. Sturhahn, and B. Chen, Phys. Earth Planet. Inter. **88**, 114 (2011).
[57]O. L. Anderson, Phys. Earth Planet. Inter. **112**, 267 (1999).
[58]C. A. Murphy, J. Jackson, W. Sturhahn, and B. Chen, Geophys. Res. Lett. **38**, L24306 (2011).
[59]D. C. Wallace, *Thermodynamics of Crystals* (Dover, New York, 1972).
[60]W. B. Holzapfel, M. Hartwig, and W. Sievers, J. Phys. Chem. Ref. Data **30**, 515 (2001).
[61]L. V. Al'tshuler, S. E. Brusnikin, and E. A. Kuz'menkov, J. Appl. Mech. Tech. Phys. **28**, 129 (1987).
[62]A. Dewaele, P. Loubeyre, F. Occelli, M. Mezouar, P. I. Dorogokupets, and M. Torrent, Phys. Rev. Lett. **97**, 215504 (2006).
[63]R. Boehler, N. von Bargen, and A. Chopelas, J. Geophys. Res. **95**, 731 (1990).
[64]J. M. Brown, J. Appl. Phys. **88**, 5496 (2000).